基于 Beamlet 变换的结构光焊缝图像线性特征提取

黄军芬， 黄继强， 黄民双， 邓双成
（北京石油化工学院 光机电装备技术重点实验室，北京 102617）

黄军芬

摘 要：鉴于以结构光为主动光源的焊缝跟踪方法可用于识别不同坡口形式的焊缝位置信息，对结构光焊缝图像进行了分析. 为有效提取图像中结构光线性特征以确定焊缝位置，引入了束波变换. 阐述了束波变换原理，开发了基于多尺度束波变换的结构光焊缝图像线性特征提取算法. 做基于最大 Beamlet 统计的检验，对结构光焊缝图像进行小尺度束波变换以确定结构光线的大致位置，缩小搜索范围；然后对图像进行大尺度束波变换确定焊缝部分结构光线的线性特征，根据线段斜率变化可确定焊缝位置. 采用该算法确定一幅结构光焊缝图像的焊缝位置的时间为 260 ms.

关键词：束波变换；线性特征；结构光焊缝图像
中图分类号：TG115.28 文献标识码：A 文章编号：0253－360X(2009)05－0089－04

0 序 言

实现焊缝自动跟踪是提高焊接生产率、优化焊缝质量的有效途径. 经过几十年的研究和实践，焊缝跟踪技术已经取得了长足的进步. 其中以结构光为主动光源的焊缝跟踪方法，因结构光的高能量、高亮度，照射到工件表面上会发生变形，由 CCD 摄取图像并经过处理后，能够识别出不同坡口形式的焊缝中心位置及其特征信息，将焊炬的三维空间控制转换为二维控制，成为一种很有前途的跟踪控制方法[1].

鉴于焊缝跟踪以结构光为主动光源时，通过 CCD 获取的图像为一条被工件表面焊缝起伏调制的结构光线，图像中常常存在由焊接飞溅及坡口端面反射结构光造成的噪声，因此选择一种适用于线性特征有效检测的分析工具对于提取结构光焊缝图像中的激光线从而确定焊缝位置有着重要意义.

为了提取线性特征，引入一种新的多尺度的分析工具——Beamlet 变换. Beamlet 变换以不同尺度、不同方向的线段作为基，图像沿基做线积分，积分值作为目标函数进行线性特征提取.

收稿日期：2008－04－07
基金项目：北京市教育委员会科技发展计划面上项目(KM200810017006)；北京市自然科学基金资助项目(4073032)；北京石油化工学院青年科研基金资助项目(N06－04)；北京石油化工学院光机电装备技术北京市重点实验室开放课题基金资助项目(KF2007－10)

1 Beamlet 变换原理

1.1 Beamlet 变换基本概念

Beamlets 产生步骤[2,3] 如下所示.

(1) 二进分割. 开始把单位正方形划分为 4 个子正方形，每个子正方形的边长是单位正方形的 1/2，每个子正方形再分为 4 个更小的子正方形，以此类推. 图 1 描述了经过 0，1，2 和 3 步分割后的子正方形.

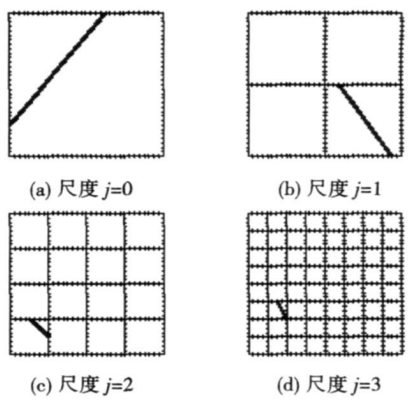

图 1 不同尺度下的 Beamlets
Fig. 1 Beamlets at different scales

(2) 标记顶点. 令固定分辨率 δ等于 1/ n，以 δ在每个子正方形的边界作标记. 即任何尺度上的子

正方形，相邻顶点的距离都是 δ的整数倍.

(3) 连接点. 在每一个子正方形里连接任何一对顶点，每条连接线段称为 Beamlet. 图 1 为位于不同尺度、位置和方向的 Beamlets，其中 j 为尺度因子.

1.2 Beamlet 变换

假设 $f(x_1, x_2)$ 为存在于单位正方形$[0, 1]^2$中的函数，函数 f 的 Beamlet 变换定义为线积分的集合

$$T_f(b) = \int_b f[x(l)]\,\mathrm{d}l,\ b \in B_{n\,\delta} \qquad (1)$$

式中：$B_{n\,\delta}$为对于$n \times n$ 图像，分辨率为 δ时，不同尺度下所有 Beamlet 的集合；线段集 b 为任一 Beamlet，如图 2 中箭头所指的 Beamlet 即为 b；$x(l)$ 为沿 b 方向 x_1, x_2 的函数；$f[x(l)]$ 为 b 上的图像函数. 称线积分 $T_f(b)$ 为对应 b 的 Beamlet 变换系数[4].

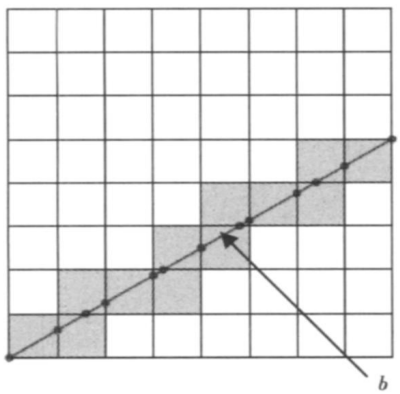

图 2 束波变换示意图

Fig. 2 Sketch map of Beamlet transform

对于实际的 $n \times n$ 图像，其图像函数 $f_{(i_1, i_2)}$ 是由 n^2 个像素组成的离散函数，故 $f_{(i_1, i_2)}$ 的 Beamlet 变换必须先通过插值得到连续函数 $f(x_1, x_2)$，然后再通过式(1)连续函数 Beamlet 变换公式得到 $T_f(b)$，$f(x_1, x_2)$ 可由插值函数求得，即

$$f(x_1, x_2) = \sum_{(i_1, i_2)} f_{(i_1, i_2)} \phi_{(i_1, i_2)}(x_1, x_2) \qquad (2)$$

式中：插值函数 $\phi_{(i_1, i_2)}$ 有多种选择，这里使用平均插值函数，即 $f_{(i_1, i_2)}$ 的取值为连续函数 $f(x_1, x_2)$ 上像素值的平均.

图2示意了将图像分成 $n \times n$ 块，用每一黑色块内灰度平均值表示束波 b 与该块相交所得顶点的灰度值，同时示意了相应的束波变换. 即束波变换为束波穿过的各方块的所有像素灰度值的加权和.

2 基于 Beamlet 变换的线性特征提取

现针对 256 像素×256 像素的结构光焊缝图像阐述基于 Beamlet 变换的线特征提取算法.

2.1 检测算法

为提取结构光焊缝图像中有用信息值，并节约运算量，做基于最大 Beamlet 统计的检验，即针对不同尺度下的每个二进方块，找到最大值，即

$$Y = T_y(b) / \sqrt{L(b)},\ b \in B_{(1/n,\,n)} \qquad (3)$$

式中：$T_y(b)$ 为数据 y 的 Beamlet 变换系数；$\sqrt{L(b)}$ 为 b(Beamlet)的几何长度；$B_{(1/n,\,n)}$ 为不同尺度下每个二进方块中的 Beamlets 的集合. 一旦 Y 超过某个阈值，将保留所有 Y 对应的 Beamlets 系数.

2.2 结构光焊缝图像线性特征提取算法

线性特征提取算法分为如下三个步骤.

(1) 图 3 为原始焊缝形貌，利用 CCD 获取结构光焊缝图像，如图 4 所示. 图中白线即为被焊缝调制了的结构光线，白线的下凹部分对应焊缝.

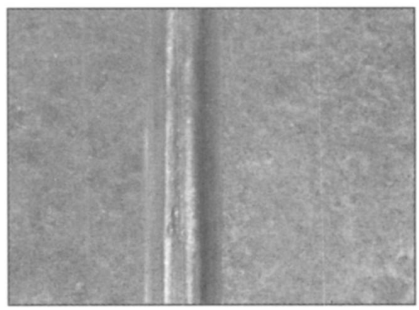

图 3 焊缝形貌

Fig. 3 Form of welding seam

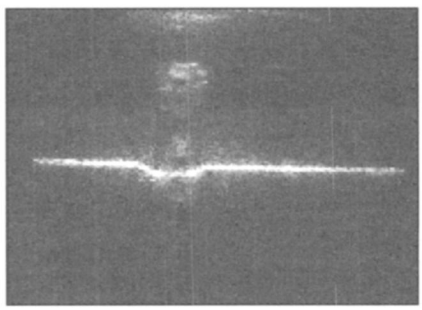

图 4 原始结构光焊缝图像

Fig. 4 Original structured light image of welding seam

(2) 对图 4 进行 0 尺度束波变换，首先标记顶点，令固定分辨率 δ等于单位像素，以 δ在结构光焊缝图像的 4 个边界作标记，标记点即为顶点；然后连接任何一对顶点，构成不同位置及方向的 Beamlet；最后进行 Beamlet 变换，根据图像的灰度分布取灰度值 100 为阈值，利用 2.1 节提出的检测算法获取 Y 值超过阈值的 Beamlets 系数.

所得计算结果如图 5 所示. 图 5a 中叠加在结构光线上的黑色线段为通过束波变化提取的线性特征位置. 图 5b 为将图 5a 中心部分放大，由图 5b 可清楚看到所提取的线性特征位置与工件表面上的结构光线吻合，但是无法反映焊缝部分（下凹部分）的结构光线. 通过该步可确定结构光线的大致位置，缩小搜索范围.

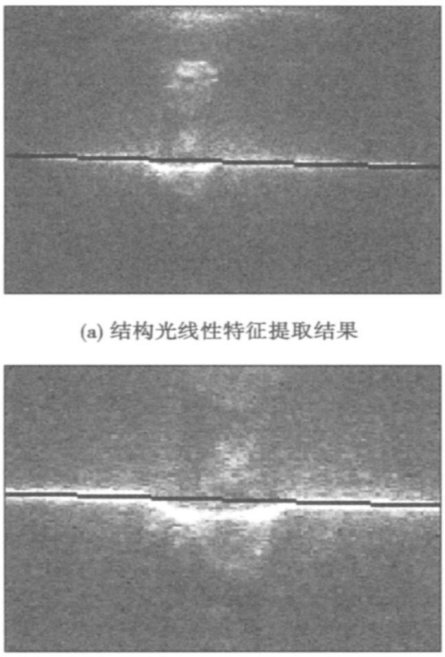

(a) 结构光线性特征提取结果

(b) 提取结果局部放大

图 5　$j=0$ 提取的结构光线信息

Fig. 5　Structured light information pickup at scale $j=0$

（3）以上一步确定的结构光线大致位置为中心缩小搜索范围致 128 像素（行数）×256 像素（列数），进行尺度为 4 的束波变换. 首先进行二进分割，即将搜索范围划分为 128 个边长为 16 像素的子正方形；对每个子正方形都要进行标记顶点、连接顶点、进行 Beamlet 变换，同样取灰度值 100 为阈值，利用 2.1 节提出的检测算法获取 Y 值超过阈值的 Beamlets 系数.

所得计算结果如图 6 所示，图 6a 中叠加在结构光线上的黑色线段即为通过束波变化提取的线性特征位置. 图 6b 为将图 6a 中心部分放大，由图 6b 可清楚看到所提取的线性特征位置与工件表面及焊缝部分（下凹部分）的结构光线均能吻合.

2.3　焊缝位置确定

由 2.2 节中算法步骤（2），即 0 尺度束波变换及相应的检测算法所提取的线性特征位置确定结构光线的大致位置及工件表面结构光线的斜率，然后通过 2.2 节中算法步骤（3）获取各子正方形中符合条件的线性特征，分别从图像左右两侧搜索线性特征——斜率发生变化的拐点，如图 6b 中两黑色圆点所示，左右拐点即对应焊缝左右边缘. 通过获取焊缝部分结构光线性特征，还可确定焊缝截面基本形貌.

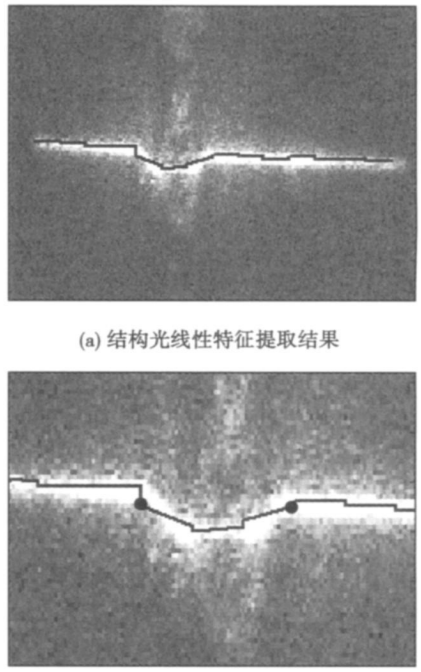

(a) 结构光线性特征提取结果

(b) 提取结果局部放大

图 6　$j=4$ 提取的结构光线信息

Fig. 6　Structured light information pickup at scale $j=4$

3　结　　论

（1）开发了一种新的提取结构光焊缝图像中结构光线线性特征的算法，该算法首先对 CCD 采集的结构光焊缝图像进行 0 尺度的束波变换，确定结构光线的大致位置及工件表面结构光线的斜率，然后对图像中包含结构光线的局部区域进行 4 尺度的束波变换，确定焊缝部分结构光线的线性特征，根据线段斜率变化可确定焊缝位置.

（2）算法的分辨率为单位像素，通过定标图像单位像素对应的空间距离可确定线性特征提取精度为 0.13 mm. 通过试验验证，提取一幅焊缝图像结构光线线性特征的时间为 260 ms，能够满足焊缝实时跟踪的要求.

参考文献：

[1]　王　伟，朱六妹，邹奇仕，等. 焊缝激光跟踪图像处理中关键技

术的研究[J]. 光电工程, 2003, 30(3): 52—55.
Wang Wei, Zhu Liumei, Zou Qishi, *et al*. Study on key techniques for image processing of seam laser tracking [J]. Opto-Electronic Engineering, 2003, 30(3): 52—55.

[2] David L Donoho, Huo Xiaoming. Beamlets and multiscale image analysis [C]// Multiscale and Multiresolution Methods. Berlin: Springer Press, 2002: 149—196.

[3] 赵金鑫, 高广珠, 余理富, 等. 基于 Beamlet 变换的图像线性特征提取[J]. 计算机仿真, 2005, 22(12): 169—173.
Zhao Jinxin, Gao Guangzhu, Yu Lifu, *et al*. Line detection in SAR imagery based on Beamlet transform [J]. Computer Simulation, 2005, 22(12): 169—173.

[4] 屈庆春, 彭玉华, 杨明强. 基于 Beamlet 变换的线特征检测[J]. 中国图象图形学报, 2007, 12(3): 500—504.
Qu Qingchun, Peng Yuhua, Yang Mingqiang. Line detection based on Beamlet transform [J]. Journal of Image and Graphics, 2007, 12(3): 500—504.

作者简介: 黄军芬, 女, 1975 年出生, 博士, 讲师. 主要从事焊缝自动识别与跟踪方面的科研和教学工作. 发表论文 20 余篇.

Email: huangjunfen@bipt.edu.cn

[上接第 88 页]

参考文献:

[1] 范希梅, 林洁琼, 杜贤昌. 陶瓷热障涂层的研究现状[J]. 长春工业大学学报, 2003, 24(1): 65—67.
Fan Ximei, Lin Jieqiong, Du Xianchang. Research progress in ceramic thermal barrier coatings[J]. Journal of Changchun University of Technology, 2003, 24(1): 65—67.

[2] 赵光岩, 饶平根, 吕 明. 莫来石及多孔莫来石的研究和应用[J]. 中国陶瓷, 2006, 42(9): 13—17.
Zhao Guangyan, Rao Pinggen, Lü Ming. Research and applications of mullite and porous mullite [J]. China Ceramic, 2006, 42(9): 13—17.

[3] 曹学强. 热障涂层材料[M]. 北京: 科学出版社, 2007.

[4] Ng H W, Gan Z. A finite element analysis technique for predicting as-sprayed residual stresses generated by the plasma spray coating process [J]. Finite Elements in Analysis and Design, 2005, 41: 1235—1254.

[5] 关振铎, 张中太, 焦金生. 无机材料物理性能[M]. 北京: 清华大学出版社, 1992.

[6] 汪刘应, 王汉功, 华绍春, 等. 多功能微弧等离子喷涂技术[J]. 焊接学报, 2006, 27(2): 81—84, 88.
Wang Liuying, Wang Hangong, Hua Shaochun, *et al*. Multi-functional micro-plasma spraying technique[J]. Transactions of the China Welding Institution, 2006, 27(2): 81—84.

作者简介: 侯平均, 男, 1974 年出生, 博士研究生, 工程师. 主要从事表面工程方面的研究. 发表论文 15 余篇.

Email: bighou@126.com

the temperature was measured. It is shown that the simulation results are in accordance with the experimental results. The present work not only provides a scientific basis for the position selection of temperature measurement, design of control method, and the analysis of welding defects, but also puts forward a method to optimize the process and improve the temperature distribution on tubes.

Key words: stainless steels; induction brazing; temperature field; finite element

Bonding process of pure copper with amorphous Cu-P interlayer

YU Weiyuan, CHEN Xueding, LU Wenjiang, WANG Yanhong (State Key Laboratory of Gansu Advanced Non-ferrous Metal Materials, Lanzhou University of Technology, Lanzhou 730050, China). p77—80

Abstract: An amorphous Cu-P solder was prepared as interlayer for bonding of pure copper. The melting behavior of amorphous solder was investigated. The bonding process for pure copper with amorphous Cu-P interlayer was studied by many means. The results indicate that the bonding process is composed of pre-solid diffusion, spreading and solid diffusion. The amorphous alloy has a good diffusion capability, so the pre-solid diffusion period is performed enough. A little number of liquid metal diffusion happens on the surface of base metal.

Key words: melt spinning; amorphous Cu base filler metal; vacuum brazing

Four-axis interpolation algorithm for automatic welding of saddle type curve weld LÜ Yan, TIAN Xincheng, XU Qing, PENG Bo (School of Control Science and Engineering, Shandong University, Jinan 250061, China). p81—84

Abstract: The principle, system structure, interpolation algorithm and its simulation of an automatic welding system for saddle-shaped curve were introduced. An automatic welding system was designed with four axes: τ, y, ρ and σ. Through the coordinated feeding of the four axes, the trajectory and pose of the welding torch can be controlled to implement the automatic welding of saddle-shaped curve weld. Based on the cinematic analysis and the principle of the space analytic geometry, the trajectory model and the welding torch pose model were established, and a four-axis interpolation algorithm for automated welding of saddle-shaped curve weld was proposed. The simulation of the algorithm shows that the algorithm has ideal trajectory and welding torch pose control precision. A direct trajectory control can be realized with this interpolation algorithm.

Key words: saddle-shaped curve; pose control; path interpolation

Mullite/metal composite thermal barrier coating deposited by micro-plasma spraying HOU Pingjun[1], HUANG Guopeng[2], WANG Hangong[1], WANG Liuying[1] (1. The Second Artillery Engineering College 501 Staff, Xi'an 710025, China; 2. The Second Artillery Military Agency in 7435 Factory, Wuhan 430060, China). p85—88, 92

Abstract: Mullite/metal thermal barrier coatings (MMCs) have been sprayed by micro-plasma spraying. The microstructure, bond strength, thermal barrier insulation and thermal shock resistance of the coatings have been investigated. The microstructure of MMC shows that mullite particles are surrounded by the metal lamellar structure. The average bond strength of the coatings is more than 30 MPa. The thermal barrier insulation of the coatings is improved with the increasing of surface temperature and the mullite fraction. At surface temperature of 1 175 ℃, the maximum thermal barrier insulation of coating is 125 ℃ with 70% mullite in the powder. The thermal shock resistance test, in which the specimens are heated up to 1 150 ℃ and then quenched in the water, shows that one of the main reasons for coating failure is substrate deformation. The thermal shock resistance of coatings is increased firstly, and decreased in succession quickly with the mullite fraction increasing, and the peak value of the thermal shock resistance is 72 times with 40% mullite fraction in the powder.

Key words: thermal barrier coatings (TBCs); micro-plasma spray; mullite; composite coating; thermal shock resistance

Abstraction of line segment characteristic from structured light image of weld seam based on Beamlet transform HUANG Junfen, HUANG Jiqiang, HUANG Minshuang, DENG Shuangcheng (Opto-Mechatronic Equipment Technology Beijing Area Major Laboratory, Beijing Institute of Petrochemical Technology, Beijing 102617, China). p89—92

Abstract: Analysis on the structured light image of weld seam was carried out since the welding seam tracking method with the structured light as an active lighting can be used to recognize the position of the weld seam with different groove shapes. The Beamlet transform was introduced to detect the line segment characteristic of the structured light in the image to identify the position of the weld seam effectively. The theory of Beamlet transform was introduced, and a line segment characteristic detection algorithm was developed for the structured light image of weld seam based on multiscale Beamlet transform. Test based on the maximal Beamlet statistics was carried out. Beamlet transform at a small scale to the structured light image of weld seam was done to identify the rough position of the structured light and reduce the searching range, and Beamlet transform at a large scale was done to identify the line segment characteristic of the structured light on the weld seam, then the weld seam position can be detected according to the slope variety of the line segments. The time to detect the position of the weld seam in a structured light image of weld seam is 260 ms by the algorithm.

Key words: Beamlet transform; line segment characteristic;

structured light image of weld seam

Elimination of gas holes of laser cladding on 2A12 aluminum alloys SUN Fujuan (Qingdao Branch, Naval Aeronautical Engineering Academy, Qingdao 266041, Shandong, China). p93—96

Abstract: Laser cladding Al-Y (6% Y) was used to repair corrosion damage of 2A12 aluminum alloys. One group of the specimens was shocked on every deposited layer, the other was only deposited Al-Y(6%Y). After aging and fatigue test, fracture and element test were studied. The results show that the safety life of the shocked specimen is 871% of the specimens without shock and there was no pore in the deposited layer which is joined firmly with the substrate. There were many pores in the deposited layer of the specimens without shock, which lead to reduction of the safety life. The element test indicates that parts of the substrate is engaged in metallurgical procedure and the element Y is seriously burnt.

Key words: aluminum alloys; laser cladding; safety life; fatigue fracture

Experiment research on laser transmission welding of two different thermoplastics WANG Xiao, YANG Kun, ZHANG Huizhong, LIU Huixia (School of Mechanical Engineering, Jiangsu University, Zhenjiang 212013, Jiangsu, China). p97—100

Abstract: The experiments on laser transmission welding of dissimilar plastic between transparent PS and PVC were carried out with clearweld additive, and the welding quality was investigated by orthogonal test. Tensile and section tests were conducted for experimental samples, and the influence of welding factors on tensile strength and weld seam size were analyzed. The optimized welding parameters are obtained by range method, which indicates the influencing parameters on welding strength are welding speed, fixture pressure, beam diameter, laser average power, laser frequency, holding time after welding. Research results are helpful to guide practical production.

Key words: laser welding; polystyrene; polyvinylchlorid; additive; transmission welding

Digital AC servo push & pull feeding system for CO_2 welding YANG Shuai, LIU Jia, YAN Sibo, YIN Shuyan (College of Mechanical Engineering & Applied Electrons Technology, Beijing University of Technology, Beijing 100124, China). p101—104

Abstract: A push & pull feeding system with real-time control for CO_2 welding was proposed and achieved. It utilizes the motion controller to control AC servo motor with the low moment of inertia, fast response, and the buffer to connect the constant feeding part and the push & pull feeding part. The PWM feeder speed control circuit with speed negative feedback by rotate coder was designed to compensate the speed fluctuation caused by the system load and supply voltage changing. The push & puller feeding mechanism was designed to push & pull the wire based on the AC servo motor. According to the characteristics of CO_2 welding with push & pull feeding system, the feeder speed curve is pre-designed. The wire motion was managed by the real-time control software written in the motion controller. The system has good ability in anti-jamming and stability. The highest feeder frequency with push & pull process can reach 90 Hz.

Key words: AC servo motor; buffer; real-time control; push & pull feeding

SPH simulation on agglomerate Fe particle deposition in low temperature high velocity air fuel spraying process HOU Genliang[1], XU Xin[2], YUAN Xiaojing[1] (1. The Second Artillery Engineering College 501 staff, Xi'an 710025, China; 2. The Second Artillery Equipment Research Institute, Beijing, 100085, China). p105—108

Abstract: In order to study the effect of the agglomerate metal particle on the coatings building-up, the agglomerate nano metal particle deposition characteristics with smoothed particle hydrodynamics (SPH) were simulated in low temperature high velocity air fuel (LTHVAF) thermal spraying process. The results show that the agglomerate particles are splashed when the agglomerate particles impact on the substrate. During the deposition process, the effective strain of agglomerate particle is larger than that of the micron particle, but the area ratio of the agglomerate particle is less. At the same time, the pervasion occurs when the metal particle impacts on the substrate, which increases with the particle velocity.

Key words: thermal spray; nano-agglomerate particle; deposition characteristics; numerical simulation

Numerical simulation of welding deformation of a large carriage side wall YAN Junxia, WANG Jun, ZHAO Chenyang, LIU Limin (College of Materials, Hebei University of Science and Technology, Shijiazhuang 050018, China). p109—112

Abstract: The main welding deformation of railway carriage side-wall was welded buckling distortion, which was simulated by thermal elastic-plastic finite element method with analysis in several selected areas including continuous welds, plug welds and intermittent welds. The results show that the plug welding and intermittent welding are the main reason that induce bucking distortion of side-wall in which transverse stiffeners and longitudinal stiffeners are welded on the side-wall. The critical bucking load decreases obviously and the bucking distortion increases on the plate with a free boundary. The measured results of bucking distortion are in agreement with the simulation results. Thus, a complete set of instruction can be received for the real processing.

Key words: carriage side-wall; numerical simulation; buckling distortion